IAA-AAS-DyCoSS2 14-14-09

LOW THRUST MINIMUM FUEL OPTIMIZATION IN THE CIRCULAR RESTRICTED THREE BODY MODEL

Chen Zhang[*], Francesco Topputo[†], Franco Bernelli-Zazzera[‡], Yu-Shan Zhao[§]

In this paper, low-thrust fuel-optimal transfer trajectories are studied in the Earth-Moon restricted three-body model with constant specific impulse engines. In order to cope with high computational burden and convergence problems caused by multi spirals and large number of bang-bang control structures, homotopy method is implemented by starting from the related and easier energy-optimal problem, for which, the analytical Jacobian is derived, and a combination of Newton and bisection methods is proposed to accurately detect the switching points together with a variable step 7th/8th-order Runge-Kutta integrator. The case study is a low-thrust transfer from the GTO to a periodic three-dimensional halo orbit around the Earth-Moon L_1 point. Initial costates are first achieved by solving the problem with a high thrust level, which is then reduced through discrete homotopy. The final orbit has about 150 revolutions and the control profile is characterized by about 150 bang-bang structures. The techniques presented in the paper are useful in practical cases where very low-thrust accelerations is used in high nonlinear vector fields.

INTRODUCTION

The fascinating properties of the restricted three-body problem have attracted much attentions since Euler and Lagrange discovered the five libration points, and since Poincare devised the dynamical system theory. In 1978, ISEE-3[1] (International Sun-Earth Explorer-3) was the first mission to fly in a halo orbit, followed by SOHO (1995)[2] (Solar and Heliospheric Observatory), ACE (1997)[3] (Advanced Composition Explorer), WMAP (2001)[4] (Wilkinson Microwave Anisotropy Probe) and Genesis (2001).[5] On the other hand, owing to the high specific impulse of electric propulsion technique, it reveals the big advantage compare to traditional chemical propulsion. NASA's Deep Space 1[6] (1998) was the first spacecraft to use electric propulsion, later applications include ESA moon exploration mission Smart-1 (2003)[7] and JAXA sample return mission HAYABUSA (2003).[8] With the development of space technology, future scientific missions not only demand better observing conditions near the Lagrange libration points, but also require lower fuel consumption and better trajectory accuracy to target these areas. In order to meet these requirements, low-thrust technique and the three-body dynamics are merged together to design transfer trajectories. The essence of low-thrust problem is optimization of a functional and it can be formulated as an optimal control problem(OCP),[9] the solution methods generally fall into two categories, direct and indirect methods, direct methods convert the OCP into parameter optimization problem through discretization and then resort to nonlinear programming.[10,11] Direct methods are generally robust and can easily

[*]Beijing University of Aeronautics and Astronautics, No.37 Xueyuan Road, Beijing, 100191, China
[†]Department of Aerospace Science and Technology, Politecnico di Milano, Via La Masa 34, Milano, 20156, Italy
[‡]Department of Aerospace Science and Technology, Politecnico di Milano, Via La Masa 34, Milano, 20156, Italy
[§]Beijing University of Aeronautics and Astronautics, No.37 Xueyuan Road, Beijing, 100191, China

implement path constraints, but they often cost large computational effort. While indirect method convert OCP to two point boundary value problem[10] (TPBVP) by calculus of variations and pontryagain minimal principle[12](PMP). This kind of method can ensure the local optimality of a converged solution, and a good start point will cause rapidly convergence, but the most difficulties are the small convergence radius and sensitive initial costates and they lack of physical meaning. Much research has been conducted on low-thrust three-body trajectory optimization. Senent[13] derived the first-order necessary conditions with variable specific impulse (VSI) engine and solved transfer trajectories to the halo orbits under Sun-Earth/Moon systems. Ozimek and Howell[14] also consider variable specific impulse engine and found the practial control law for transfers under Earth-Moon models. Relying on direct transcription and collocation approach, Mingotti and Topputo[15,16,17] solved transfer trajectories under Earth-Moon models using constant specific impulse engines. Caillau[18] also considered constant specific impulse engine transfers from GEO to Earth-Moon L_1 libration point and to an orbit around Moon respectively, in his work, homotopic method is used to link the difficult fuel-optimal problem with the more easier energy-optimal problem. Russell[19] derived the analytical Jacobian of shooting constraints and extend the three-body low-thrust transfer to Jupiter-Europa system. This paper will emphasis on a more practical GTO to Earth-Moon Halo transfer with indirect method and constant specific impulse engine, some effective techniques are presented to cope with convergence and sensitivity problem arising from the multi-spirals and large number of bang-bang structures.

The paper is organised as follows: In Section 1, the dynamical model is presented, then the shooting functions are derived with respect to fuel-optimal, energy-optimal and time-optimal problems. In Section 2, the analytical Jacobian for both energy-optimal and fuel-optimal problems are derived. In Section 3, a combination of Newton and bisection method is sketched to detect switching points. In Section 4, the techniques stated above are applied to solve low-thrust transfer GTO to Earth-Moon L_1 transfer trajectory.

DYNAMICAL MODELS

The controlled motion of a spacecraft under the influence of two primaries is described in this section using the circular restricted three-body problem.

Circular restricted three-body problem (CRTBP)

The circular restricted three-body problem[20](CRTBP) studies the motion of a massless spacecraft m_3 under the gravitational field generated by the mutual circular motion of two primaries of m_1 and m_2 respectively, about their common center of mass. The dynamics is written in rotating frame with non-dimensional units: the angular velocity of m_1, m_2, their distance, and the sum of their masses are all set to 1, then $\mu = m_2/(m_1 + m_2)$ is the only mass parameter of the system. The Earth-Moon CRTBP is studied in this work, for which $\mu = 0.01215$. It is easy to verify that Earth of mass $(1 - \mu)$, is located at $(-\mu, 0, 0)$, whereas Moon of mass μ, is located at $(1 - \mu, 0, 0)$. To model the controlled motion of spacecraft under both gravitational attractions of Earth, Moon and the low-thrust propulsion, the following differential equations are considered

$$\dot{\boldsymbol{x}} = \boldsymbol{f}(\boldsymbol{x}, \boldsymbol{\alpha}, u) \Rightarrow \begin{bmatrix} \dot{\boldsymbol{r}} \\ \dot{\boldsymbol{v}} \\ \dot{m} \end{bmatrix} = \begin{bmatrix} \boldsymbol{v} \\ \boldsymbol{g}(\boldsymbol{r}) + \boldsymbol{h}(\boldsymbol{v}) + \frac{T_{max}u}{m}\boldsymbol{\alpha} \\ -\frac{T_{max}u}{c} \end{bmatrix} \tag{1}$$

where $\boldsymbol{r} = [x, y, z]^T$ and $\boldsymbol{v} = [v_x, v_y, v_z]^T$ respectively, m denotes the instantaneous mass of spacecraft, T_{max} is the maximal thrust magnitude, $c = I_{sp} g_0$ represent exhaust velocity, (I_{sp} is the thruster specific impulse and g_0 is the gravitational acceleration at the sea level). The control variables are the engine thrust ratio, $u \in [0, 1]$, and the unit vector of thrust direction $\boldsymbol{\alpha}$. $\boldsymbol{g}(\boldsymbol{r})$ and $\boldsymbol{h}(\boldsymbol{v})$ are defined as functions of position and velocity in the synodic reference frame respectively,

$$\boldsymbol{g}(\boldsymbol{r}) = \begin{bmatrix} x - \frac{(1-\mu)(x+\mu)}{r_1^3} - \frac{\mu(x+\mu-1)}{r_2^3} \\ y - \frac{(1-\mu)y}{r_1^3} - \frac{\mu y}{r_2^3} \\ -\frac{(1-\mu)z}{r_1^3} - \frac{\mu z}{r_2^3} \end{bmatrix}, \boldsymbol{h}(\boldsymbol{v}) = \begin{bmatrix} 2v_y \\ -2v_x \\ 0 \end{bmatrix} \tag{2}$$

where r_1 and r_2 represent the distance of m_3 to the Earth and Moon, respectively

$$\begin{aligned} r_1 &= \left[(x+\mu)^2 + y^2 + z^2\right]^{\frac{1}{2}} \\ r_2 &= \left[(x+\mu-1)^2 + y^2 + z^2\right]^{\frac{1}{2}} \end{aligned} \tag{3}$$

Energy-optimal problem and homotopic method

The performance index used to minimize the fuel consumption is expressed by[21]

$$J_f = \frac{T_{max}}{c} \int_{t_0}^{t_f} u \, \mathrm{d}t \tag{4}$$

Where t_0 and t_f denote the initial and final time respectively. However, several articles pointed out that for fuel-optimal problem, the thrust magnitude is piece-wise continuous and it will perform either zero or maximum.[22] This 'bang-bang' attribute cause discontinuous dynamics and if indirect method is implemented, the corresponding shooting function is difficult to solve directly by single shooting method.[23] Bertrand[24] introduced smoothcing techniques also called homotopic approach to overcome these difficulties. In this work a named energy-consumption homotopy will link the related and easier energy-optimal problem (i.e., L^2-norm of control) to the difficult fuel-optimal problem[23] (i.e., L^1-norm of control) by a parameter ε. The new performance index read

$$J_e = \frac{T_{max}}{c} \int_{t_0}^{t_f} \left[u - \varepsilon u(1-u)\right] \, \mathrm{d}t, \varepsilon \in [0, 1] \tag{5}$$

When $\varepsilon = 1$, the above performance index is energy-optimal problem, while $\varepsilon = 0$ it will return to the fuel-optimal problem. Suppose the satellite start from a fixed point on the GTO and target another point located on the periodic orbit of L_1 in the Earth-Moon system with free final mass. The transfer trajectory should subject to the following boundary conditions

$$\boldsymbol{\psi}_0 = \begin{bmatrix} \boldsymbol{r}(t_0) - \boldsymbol{r}_0 \\ \boldsymbol{v}(t_0) - \boldsymbol{v}_0 \\ m(t_0) - 1 \end{bmatrix} = 0 \tag{6}$$

$$\boldsymbol{\psi}_f = \begin{bmatrix} \boldsymbol{r}(t_f) - \boldsymbol{r}_f \\ \boldsymbol{v}(t_f) - \boldsymbol{v}_f \end{bmatrix} = 0 \tag{7}$$

and the constraints on the controls are given

$$\begin{aligned} \boldsymbol{\alpha}^T\boldsymbol{\alpha} - 1 = 0 \\ u - \sin\sigma^2 = 0 \end{aligned} \tag{8}$$

The first constraint indicates that $\boldsymbol{\alpha}$ is a vector of unit magnitude, and the second constraint use the unbound slack variable σ to force the engine thrust magnitude ratio between $[0, 1]$. Next, J_e is augmented into an unconstrained optimization function J_e' by adjoining the Lagrange multipliers $\boldsymbol{\nu}_0 = [\boldsymbol{\nu}_{r_0}, \boldsymbol{\nu}_{v_0}, \nu_{m_0}]^T$ and $\boldsymbol{\nu}_f = [\boldsymbol{\nu}_{r_f}, \boldsymbol{\nu}_{v_f}]^T$ to the boundary conditions, the time-varying costates $\boldsymbol{\lambda} = [\boldsymbol{\lambda}_r, \boldsymbol{\lambda}_v, \lambda_m]^T$ to the dynamical constraints (i.e., Eq. (1)) as well as Lagrange multipliers η_1 and η_2 to the dynamic constraints of controls, respectively[14,25]

$$\begin{aligned} J_e' &= \boldsymbol{\nu}_0^T\boldsymbol{\psi}_0 + \boldsymbol{\nu}_f^T\boldsymbol{\psi}_f + \int_{t_0}^{t_f} \left[L + \boldsymbol{\lambda}^T(\boldsymbol{f} - \dot{\boldsymbol{x}}) + \eta_1(\boldsymbol{\alpha}^T\boldsymbol{\alpha} - 1) + \eta_2(u - \sin\sigma^2)\right] \mathrm{d}t \\ &= \boldsymbol{\nu}_0^T\boldsymbol{\psi}_0 + \boldsymbol{\nu}_f^T\boldsymbol{\psi}_f + \int_{t_0}^{t_f} \left[H + \dot{\boldsymbol{\lambda}}^T\boldsymbol{x} + \eta_1(\boldsymbol{\alpha}^T\boldsymbol{\alpha} - 1) + \eta_2(u - \sin\sigma^2)\right] \mathrm{d}t - \boldsymbol{\lambda}^T\boldsymbol{x}|_{t_0}^{t_f} \\ &= \Psi + \int_{t_0}^{t_f} \left[H' + \dot{\boldsymbol{\lambda}}^T\boldsymbol{x}\right] \mathrm{d}t - \boldsymbol{\lambda}^T\boldsymbol{x}|_{t_0}^{t_f} \end{aligned} \tag{9}$$

where $\Psi = \boldsymbol{\nu}_0^T\boldsymbol{\psi}_0 + \boldsymbol{\nu}_f^T\boldsymbol{\psi}_f$ and H denote the hamiltonian function, which is given by

$$H = L + \boldsymbol{\lambda}^T\boldsymbol{f} = \frac{T_{max}}{c}\left[u - \varepsilon u(1-u)\right] + \boldsymbol{\lambda}_r^T\boldsymbol{v} + \boldsymbol{\lambda}_v^T\left(\boldsymbol{g}(\boldsymbol{r}) + \boldsymbol{h}(\boldsymbol{v}) + \frac{T_{max}u}{m}\boldsymbol{\alpha}\right) - \lambda_m\frac{T_{max}u}{c} \tag{10}$$

In addition, H' is the augmented hamiltonian function, which read

$$H' = H + \eta_1(\boldsymbol{\alpha}^T\boldsymbol{\alpha} - 1) + \eta_2(u - \sin\sigma^2) \tag{11}$$

suppose the initial and final times are fixed, a local minimum of J_e' is available by nulling the total first-order variation

$$\begin{aligned} \delta J_e' = &\left(\frac{\partial\Psi}{\partial\boldsymbol{x}_0}\right)^T\delta\boldsymbol{x}_0 + \left(\frac{\partial\Psi}{\partial\boldsymbol{x}_f}\right)^T\delta\boldsymbol{x}_f + \left(\frac{\partial\Psi}{\partial\boldsymbol{\nu}_0}\right)^T\delta\boldsymbol{\nu}_0 + \left(\frac{\partial\Psi}{\partial\boldsymbol{\nu}_f}\right)^T\delta\boldsymbol{\nu}_f + \int_{t_0}^{t_f}\left[\left(\frac{\partial H'}{\partial\boldsymbol{x}}\right)^T\delta\boldsymbol{x}\right. \\ &\left. + \dot{\boldsymbol{\lambda}}^T\delta\boldsymbol{x} + \left(\frac{\partial H'}{\partial\boldsymbol{u}}\right)^T\delta\boldsymbol{u} + \left(\frac{\partial H'}{\partial\boldsymbol{\alpha}}\right)^T\delta\boldsymbol{\alpha} + \frac{\partial H'}{\partial\sigma}\delta\sigma + \frac{\partial H'}{\partial\eta_1}\delta\eta_1 + \frac{\partial H'}{\partial\eta_2}\delta\eta_2\right]\mathrm{d}t - \boldsymbol{\lambda}_f^T\delta\boldsymbol{x}_f + \boldsymbol{\lambda}_0^T\delta\boldsymbol{x}_0 \end{aligned} \tag{12}$$

From the above equation, it can be seen that the costate dynamics are given by

$$\dot{\boldsymbol{\lambda}} = -\frac{\partial H}{\partial\boldsymbol{x}} \Longrightarrow \begin{bmatrix}\dot{\boldsymbol{\lambda}}_r \\ \dot{\boldsymbol{\lambda}}_v \\ \dot{\lambda}_m\end{bmatrix} = \begin{bmatrix}-\boldsymbol{G}^T\boldsymbol{\lambda}_v \\ -\boldsymbol{\lambda}_r - \boldsymbol{H}^T\boldsymbol{\lambda}_v \\ -\|\boldsymbol{\lambda}_v\|\frac{T_{max}u}{m^2}\end{bmatrix} \tag{13}$$

where the gradients $\boldsymbol{G}$ and $\boldsymbol{H}$ are given by

$$\boldsymbol{G} = \frac{\partial\boldsymbol{g}(\boldsymbol{r})}{\partial\boldsymbol{r}} \tag{14}$$

$$
\begin{aligned}
\boldsymbol{G}(1,1) = &\ 1-\tfrac{1-\mu}{r_1^3}+\tfrac{3(1-\mu)(x+\mu)^2}{r_1^5}-\tfrac{\mu}{r_2^3}+\tfrac{3\mu(x+\mu-1)^2}{r_2^5}\\
\boldsymbol{G}(1,2)=\boldsymbol{G}(2,1) = &\ \tfrac{3(1-\mu)y(x+\mu)}{r_1^5}+\tfrac{3\mu y(x+\mu-1)}{r_2^5}\\
\boldsymbol{G}(1,3)=\boldsymbol{G}(3,1) = &\ \tfrac{3(1-\mu)z(x+\mu)}{r_1^5}+\tfrac{3\mu z(x+\mu-1)}{r_2^5}\\
\boldsymbol{G}(2,2) = &\ 1-\tfrac{1-\mu}{r_1^3}+\tfrac{3(1-\mu)y^2}{r_1^5}-\tfrac{\mu}{r_2^3}+\tfrac{3\mu y^2}{r_2^5}\\
\boldsymbol{G}(2,3) = &\ \tfrac{3(1-\mu)yz}{r_1^5}+\tfrac{3\mu yz}{r_2^5}\\
\boldsymbol{G}(3,3) = &\ -\tfrac{1-\mu}{r_1^3}+\tfrac{3(1-\mu)z^2}{r_1^5}-\tfrac{\mu}{r_2^3}+\tfrac{3\mu z^2}{r_2^5}
\end{aligned}
$$

$$
\boldsymbol{H}=\frac{\partial \boldsymbol{h}(\boldsymbol{v})}{\partial \boldsymbol{v}}=\begin{bmatrix}0 & 2 & 0\\ -2 & 0 & 0\\ 0 & 0 & 0\end{bmatrix} \tag{15}
$$

In addition, some other relations are derived from Eq. (12)

$$
\frac{\partial H'}{\partial \boldsymbol{\alpha}}=\boldsymbol{\lambda}_v\frac{T_{max}u}{m}+2\eta_1\boldsymbol{\alpha}=0 \tag{16}
$$

$$
\frac{\partial H'}{\partial \sigma}=-\eta_2\sin\sigma\cos\sigma=0 \tag{17}
$$

$$
\begin{cases}
\dfrac{\partial H'}{\partial \eta_1}=\boldsymbol{\alpha}^T\boldsymbol{\alpha}-1=0\\
\dfrac{\partial H'}{\partial \eta_2}=u-T_{max}\sin\sigma^2=0
\end{cases} \tag{18}
$$

$$
\begin{cases}
\dfrac{\partial \boldsymbol{\Psi}}{\partial \boldsymbol{\nu}_0}=\boldsymbol{\psi}_0=0\\
\dfrac{\partial \boldsymbol{\Psi}}{\partial \boldsymbol{\nu}_f}=\boldsymbol{\psi}_f=0
\end{cases} \tag{19}
$$

$$
\begin{cases}
\boldsymbol{\lambda}_0=-\dfrac{\partial \boldsymbol{\Psi}}{\partial \boldsymbol{x}_0}=-\boldsymbol{\nu}_0\\
\boldsymbol{\lambda}_f=\dfrac{\partial \boldsymbol{\Psi}}{\partial \boldsymbol{x}_f}=[\boldsymbol{\nu}_{r_f},\boldsymbol{\nu}_{v_f},0]^T
\end{cases} \tag{20}
$$

Eq. (16) indicates that $\boldsymbol{\alpha}$ is parallel to $\boldsymbol{\lambda}_v$ and Eq. (8) tells that $\boldsymbol{\alpha}$ is a unit vector, so the two possible cases are $\boldsymbol{\alpha}=\boldsymbol{\lambda}_v/\|\boldsymbol{\lambda}_v\|$ or $\boldsymbol{\alpha}=-\boldsymbol{\lambda}_v/\|\boldsymbol{\lambda}_v\|$. In addition, Pontryagain-Minimum-Principle[12](PMP) pointed out that the control should minimize hamiltonian at all points along the time history, it is clear that the optimal thrust direction is given by

$$
\boldsymbol{\alpha}^*=-\frac{\boldsymbol{\lambda}_v}{\|\boldsymbol{\lambda}_v\|} \tag{21}
$$

The above equation also known as prime vector theory.[26] Eq. (18) and Eq. (19) are constraints of controls and boundary conditions respectively. Eq. (20) also called transversality condition, because $\boldsymbol{\lambda}_0$, $\boldsymbol{\lambda}_f$, $\boldsymbol{\nu}_0$ and $\boldsymbol{\nu}_f$ are all unknown lagrange multipliers, the only useful information is $\lambda_m(t_f)=0$. Substituting Eq. (21) into Eq. (10) and recollect hamiltonian function, which is given

$$
H_e=\boldsymbol{\lambda}_r^T\boldsymbol{v}+\boldsymbol{\lambda}_v^T\left(\boldsymbol{g}(\boldsymbol{r})+\boldsymbol{h}(\boldsymbol{v})\right)+\frac{T_{max}}{c}u\left(S_e-\varepsilon+\varepsilon u\right) \tag{22}
$$

where a switching function S_e is defined

$$S_e = -\|\boldsymbol{\lambda}_v\|\frac{c}{m} - \lambda_m + 1 \tag{23}$$

and the first order derivative of switching function can be derived as follow

$$\dot{S}_e = \frac{c}{m}\frac{(-\boldsymbol{\lambda}_r - \boldsymbol{H}^T\boldsymbol{\lambda}_v)\cdot\boldsymbol{\lambda}_v}{\|\boldsymbol{\lambda}_v\|} \tag{24}$$

Once a set of canonical variables ($i.e.$, $\boldsymbol{y} = [\boldsymbol{x}, \boldsymbol{\lambda}]^T$) are given, u is the only variable in Eq. (22). It can be found that the last part of Eq. (22) is a quadratic function of u and two roots are $u_1 = 0$ and $u_2 = (\varepsilon - S_e)/\varepsilon$ respectively, in order to minimize the hamiltonian $H_e(u)$ along time history, the PMP is used again to choose the optimal thrust magnitude ratio u^* between the feasible region (i.e., [0,1]). As illustrated in Fig. 1 there are three cases of u^* depending on the different locations of u_2, which is concluded in Eq. (25) and illustrated in Fig. 1

$$u^* = \begin{cases} 0, & \text{if} \quad u_2 < 0 \\ (\varepsilon - S_e)/2\varepsilon, & \text{if} \quad 0 \le u_2 \le 2 \\ 1, & \text{if} \quad u_2 > 2 \end{cases} \tag{25}$$

Take $u_2 = (\varepsilon - S_e)/\varepsilon$ into Eq. (25), the relation between u^* and switching function S_e are given

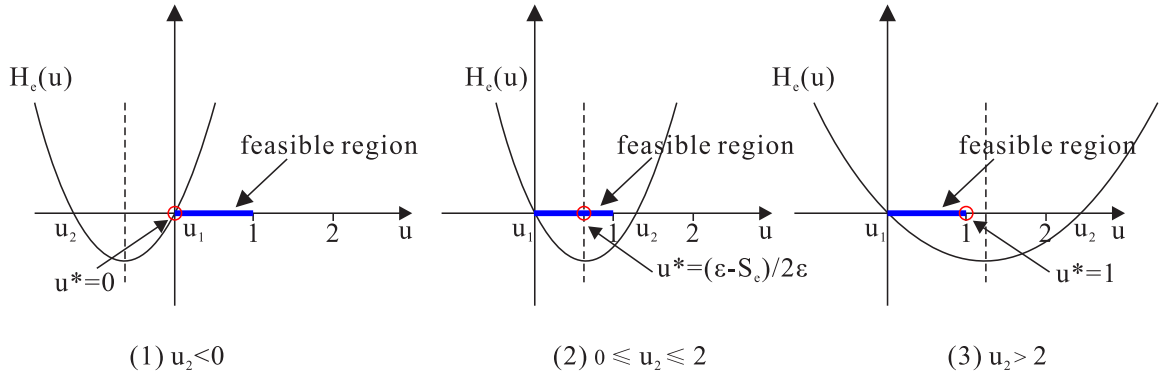

Figure 1. Optimal thrust magnitude ratio u^* with respect to different location of u_2

in Eq. (26) and illustrated in Fig. 2

$$u^* = \begin{cases} 0, & \text{if} \quad S_e > \varepsilon \\ (\varepsilon - S_e)/2\varepsilon, & \text{if} \quad -\varepsilon \le S_e \le \varepsilon \\ 1, & \text{if} \quad S_e < -\varepsilon \end{cases} \tag{26}$$

Substitute the control relation Eq. (21) into the state equations Eq. (1) to obtain the (state and costate) canonical system of equations

$$\dot{\boldsymbol{y}} = \boldsymbol{f}'(\boldsymbol{x}, \boldsymbol{\lambda}) \Rightarrow \begin{bmatrix} \dot{\boldsymbol{r}} \\ \dot{\boldsymbol{v}} \\ \dot{m} \\ \dot{\boldsymbol{\lambda}}_r \\ \dot{\boldsymbol{\lambda}}_v \\ \dot{\lambda}_m \end{bmatrix} = \begin{bmatrix} \boldsymbol{v} \\ \boldsymbol{g}(\boldsymbol{r}) + \boldsymbol{h}(\boldsymbol{v}) - \frac{\boldsymbol{\lambda}_v}{\|\boldsymbol{\lambda}_v\|}\frac{T_{max}u}{m} \\ -\frac{T_{max}u}{c} \\ -\boldsymbol{G}^T\boldsymbol{\lambda}_v \\ -\boldsymbol{\lambda}_r - \boldsymbol{H}^T\boldsymbol{\lambda}_v \\ -\|\boldsymbol{\lambda}_v\|\frac{T_{max}u}{m^2} \end{bmatrix} \tag{27}$$

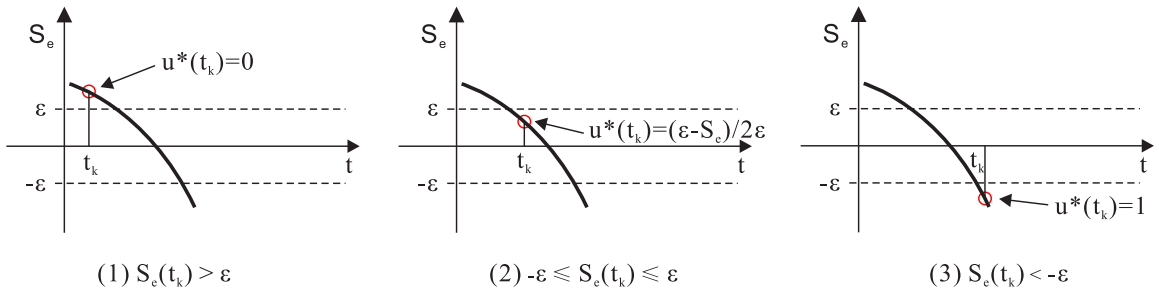

Figure 2. Optimal thrust magnitude ratio u^* with respect to the time-varying S_e

The states and costates are lumped into a single vector $\boldsymbol{y} = [\boldsymbol{x}, \boldsymbol{\lambda}]^T$ for convenience, and denote $\boldsymbol{f}'(\boldsymbol{x}, \boldsymbol{\lambda})$ as the augmented dynamics in order to distinguish from Eq. (1). And as stated above, the initial state variables (i.e., $\boldsymbol{x}_0$) are fixed, once given the initial costates (i.e., $\boldsymbol{\lambda}_0 = [\boldsymbol{\lambda}_r(t_0), \boldsymbol{\lambda}_v(t_0), \lambda_m(t_0)]^T$), the final states and costates can be obtained by integrating Eq. (27) with implicit optimal control law Eq. (21) and Eq. (26). Now, the optimal control problem can be converted to a TPBVP which consist in finding 7 unknown initial costates in order to satisfy 7 boundary equality constraints, the corresponding shooting function $Z_e(\boldsymbol{\lambda}_0)$ is written as below.

$$Z_e(\boldsymbol{\lambda}_0) \mapsto \begin{bmatrix} \boldsymbol{r}(t_f) - \boldsymbol{r}_f \\ \boldsymbol{v}(t_f) - \boldsymbol{v}_f \\ \lambda_m(t_f) \end{bmatrix} = 0 \tag{28}$$

Noted that this kind of method can ensure the local optimality of objective function if the shooting process converged. Once obtain the solution of the energy-optimal problem, let the parameter ε of Eq. (5) decrease by a certain series, and take the converged initial costates in the current step as the initialization of the next step, finally the corresponding fuel-optimal solution can be obtained. Noted that in Fig. 2, if $\epsilon = 0$, the magnitude of optimal thrust ratio u^* only depend on the sign of switching function S_e, that is to say, $u^* = 1$ when S_e is negative and $u^* = 0$ when S_e is positive.

Time-optimal problem

Though the aim of this work is fuel-optimal problem, time-optimal problem[18] is also mentioned in order to fix the transfer time $t_f \geq t_{f_{min}}$. The performance index of time-optimal problem is read

$$J_t = \int_{t_0}^{t_f} 1 \, \mathrm{d}t \tag{29}$$

the hamiltonian of time-optimal problem can be built by introducing the Lagrange multipliers

$$H_t = \boldsymbol{\lambda}_r^T \boldsymbol{v} + \boldsymbol{\lambda}_v^T \left(\boldsymbol{g}(\boldsymbol{r}) + \boldsymbol{h}(\boldsymbol{v}) + \frac{T_{max} u}{m} \boldsymbol{\alpha} \right) - \lambda_m \frac{T_{max} u}{c} + 1 \tag{30}$$

with the help of PMP, the optimal thrust magnitude ratio are given

$$u^* = \begin{cases} u = 0, & \text{if } S_t > 0 \\ u \in [0, 1], & \text{if } S_t = 0 \\ u = 1, & \text{if } S_t < 0 \end{cases} \tag{31}$$

where switching function of time optimal is denoted as S_t, which is given

$$S_t = -\|\boldsymbol{\lambda}_v\|\frac{c}{m} - \lambda_m \tag{32}$$

Noted that the switching function of time-optimal problem is different from Eq. (23). The transversality condition tells that when the final time is free, the corresponding hamiltonian $H_t(t_f)$ should be zero. Now there are 8 unknowns and 8 equality constraints, the time-optimal problem can be transformed to the corresponding TPBVP problem and the following shooting function $Z_t(\boldsymbol{\lambda}_0, t_f)$ must be satisfied.

$$Z_t(\boldsymbol{\lambda}_0, t_f) \mapsto \begin{bmatrix} \boldsymbol{r}(t_f) - \boldsymbol{r}_f \\ \boldsymbol{v}(t_f) - \boldsymbol{v}_f \\ \lambda_m(t_f) \\ H_t(t_f) \end{bmatrix} = 0 \tag{33}$$

ANALYTIC DERIVATIVES

As stated previously, the optimal control problem is transformed to TPBVP and then solved with shooting method. The related Newton-type nonlinear algorithm base on a simple idea. We want to make slight adjustments of the shooting variables so that an adjusted trajectory will target the final boundary constrains, but these algorithms are known to be very sensitive to the initialization point especially for long time transfer problem, so the analytic derivatives rather than finite-differences are used to afford gradient information for both efficiency and robustness consideration. Analytic partial derivatives are calculated using the state transition matrix $\boldsymbol{\Phi}$, which is equivalent to the partial derivative of the final states with respect to the initial states. Some properties of state transition matrix are given below

$$\begin{aligned} &\boldsymbol{\Phi}(t, t_0) = \tfrac{\partial \boldsymbol{y}(t)}{\partial \boldsymbol{y}(t_0)} \\ &\dot{\boldsymbol{\Phi}}(t, t_0) = \left.\tfrac{\partial \boldsymbol{f}'}{\partial \boldsymbol{y}}\right|_t \boldsymbol{\Phi}(t, t_0) \\ &\boldsymbol{\Phi}(t_0, t_0) = \boldsymbol{I}_{14\times 14} \end{aligned} \tag{34}$$

It is noted that in Eq. (34), Jacobian matrix of the flow field (i.e., $(\partial \boldsymbol{f}'/\partial \boldsymbol{y})\big|_t$) is time dependent and the state transition matrix $\boldsymbol{\Phi}$ should be numerically integrated along the reference trajectory from t_0 to t. When combined with 14 first-order equations of Eq. (27), a set of $14^2 + 14 = 210$ differential equations require simultaneously integration for computing $\boldsymbol{\Phi(t, t_0)}$. However, as illustrated in Fig. 2 and Eq. (34), the dynamics of state transition matrix are different depending on the region of S_e. In more detail, if the thruster always turn 'On' or 'Off' (i.e., $u^* = 1$ or $u^* = 0$) within an integration interval, the Jacobian matrix of flow field is given[19]

$$\frac{\partial \boldsymbol{f}'}{\partial \boldsymbol{y}} = \begin{bmatrix} 0 & \boldsymbol{I} & 0 & 0 & 0 & 0 \\ \boldsymbol{G} & \boldsymbol{H} & \frac{\boldsymbol{\lambda}_v}{\|\boldsymbol{\lambda}_v\|}\frac{T_{max}u}{m^2} & 0 & -\frac{T_{max}u}{m}\left(\frac{\boldsymbol{I}}{\|\boldsymbol{\lambda}_v\|} - \frac{\boldsymbol{\lambda}_v\boldsymbol{\lambda}_v^T}{\|\boldsymbol{\lambda}_v\|^3}\right) & 0 \\ 0 & 0 & 0 & 0 & 0 & 0 \\ -\frac{\partial(\boldsymbol{G}^T\boldsymbol{\lambda}_v)}{\partial \boldsymbol{r}} & 0 & 0 & 0 & -\boldsymbol{G}^T & 0 \\ 0 & -\frac{\partial(\boldsymbol{H}^T\boldsymbol{\lambda}_v)}{\partial \boldsymbol{v}} & 0 & -\boldsymbol{I} & -\boldsymbol{H}^T & 0 \\ 0 & 0 & 2\|\boldsymbol{\lambda}_v\|\frac{T_{max}u}{m^3} & 0 & -\frac{\boldsymbol{\lambda}_v^T}{\|\boldsymbol{\lambda}_v\|}\frac{T_{max}u}{m^2} & 0 \end{bmatrix} \tag{35}$$

But if the thruster always turn 'Medium' (i.e., $u^* = (\varepsilon - S_e)/2\varepsilon$) within an integration interval. Recall Eq. (23) and Eq. (26), in this case u^* is a function of $\boldsymbol{\lambda}_v$, m and λ_m, so the Jacobian matrix

of the flow field is derived by the chain rule

$$\frac{\partial \boldsymbol{f}'}{\partial \boldsymbol{y}} = \begin{bmatrix} 0 & \boldsymbol{I} & 0 & 0 & 0 & 0 \\ \boldsymbol{G} & \boldsymbol{H} & \Phi(2,3) & 0 & \Phi(2,5) & \Phi(2,6) \\ 0 & 0 & \Phi(3,3) & 0 & \Phi(3,5) & \Phi(3,6) \\ -\frac{\partial(\boldsymbol{G}^T\boldsymbol{\lambda}_v)}{\partial \boldsymbol{r}} & 0 & 0 & 0 & -\boldsymbol{G}^T & 0 \\ 0 & -\frac{\partial(\boldsymbol{H}^T\boldsymbol{\lambda}_v)}{\partial \boldsymbol{v}} & 0 & -\boldsymbol{I} & -\boldsymbol{H}^T & 0 \\ 0 & 0 & \Phi(6,3) & 0 & \Phi(6,5) & \Phi(6,6) \end{bmatrix} \tag{36}$$

$$\begin{cases} \Phi(2,3) = -\frac{\boldsymbol{\lambda}_v}{\|\boldsymbol{\lambda}_v\|} T_{max}\left(-\frac{u}{m^2} + \frac{\partial u}{\partial m}\right) \\ \Phi(2,5) = -\frac{T_{max}}{m}\left(\frac{\partial u}{\partial \boldsymbol{\lambda}_v}\frac{\boldsymbol{\lambda}_v}{\|\boldsymbol{\lambda}_v\|} + u\left(\frac{\boldsymbol{I}}{\|\boldsymbol{\lambda}_v\|} - \frac{\boldsymbol{\lambda}_v\boldsymbol{\lambda}_v^T}{\|\boldsymbol{\lambda}_v\|^3}\right)\right) \\ \Phi(2,6) = -\frac{\boldsymbol{\lambda}_v}{\|\boldsymbol{\lambda}_v\|}\frac{T_{max}}{m}\frac{\partial u}{\partial \lambda_m} \\ \Phi(3,3) = -\frac{T_{max}}{c}\frac{\partial u}{\partial m} \\ \Phi(3,5) = -\frac{T_{max}}{c}\frac{\partial u}{\partial \boldsymbol{\lambda}_v} \\ \Phi(3,6) = -\frac{T_{max}}{c}\frac{\partial u}{\partial \lambda_m} \\ \Phi(6,3) = -\|\boldsymbol{\lambda}_v\| T_{max}\left(-\frac{2u}{m^3} + \frac{1}{m^2}\frac{\partial u}{\partial m}\right) \\ \Phi(6,5) = -\frac{T_{max}}{m^2}\left(\frac{\boldsymbol{\lambda}_v^T}{\|\boldsymbol{\lambda}_v\|}u + \|\lambda_v\|\frac{\partial u}{\partial \boldsymbol{\lambda}_v}\right) \\ \Phi(6,6) = -\|\boldsymbol{\lambda}_v\|\frac{T_{max}}{m^2}\frac{\partial u}{\partial \lambda_m} \end{cases} \quad and \begin{cases} \frac{\partial u}{\partial m} = -\frac{\|\boldsymbol{\lambda}_v\|}{m^2}\frac{c}{2\varepsilon} \\ \frac{\partial u}{\partial \boldsymbol{\lambda}_v} = \frac{\boldsymbol{\lambda}_v^T}{\|\boldsymbol{\lambda}_v\|}\frac{c}{2\varepsilon m} \\ \frac{\partial u}{\partial \lambda_m} = \frac{1}{2\varepsilon} \end{cases} \tag{37}$$

The state transition matrix maps the perturbations along continued trajectory, however if there is a discontinuity of the dynamics within an integration interval, the switching point must be precisely detected and the changing of state transition matrix should be considered. Denote state transition matrix of switching point as $\boldsymbol{\Psi(t)}$, which is given below[19]

$$\boldsymbol{\Psi(t)} = \frac{\partial \boldsymbol{y}(t^+)}{\partial \boldsymbol{y}(t^-)} = \boldsymbol{I}_{14\times 14} + (\dot{\boldsymbol{y}}|_{t^+} - \dot{\boldsymbol{y}}|_{t^-})\left(\frac{\partial S}{\partial \boldsymbol{y}}\frac{1}{\dot{S}}\right)\Big|_{t^-} \tag{38}$$

where t^- represent the time left before the switching point, similarly t^+ is the time right after the switching point. Remember that $\boldsymbol{\Phi}$ denote the state transition matrix of continued trajectory while $\boldsymbol{\Psi}$ is the state transition matrix of discontinued points. Suppose there are N switching points, the Jacobian of final states with respect to initial states is a 14×14 dimensional matrix, and it can be calculated by multiplying each subsection together, which is given

$$\frac{\partial \boldsymbol{y}(t_f)}{\partial \boldsymbol{y}(t_0)} = \boldsymbol{\Phi}(t_f, t_0) = \boldsymbol{\Phi}(t_f, t_N^+)\boldsymbol{\Psi}_N\boldsymbol{\Phi}(t_N^-, t_{N-1}^+)\boldsymbol{\Psi}_{N-1}\ldots\boldsymbol{\Phi}(t_2^-, t_1^+)\boldsymbol{\Psi}_1\boldsymbol{\Phi}(t_1^-, t_0) \tag{39}$$

SWITCHING DETECTION TECHNIQUES

It has been mentioned that the discontinued right-hand side of Eq. (27) will cause sensitivity problem of shooting process.[23] Even small integration step size are used in variable step Runge-Kutta

propagator, integration error will accumulate and magnify at each switching point especially when long duration transfer problem is encountered. In this work, a switching detection technique combined with variable step 7th/8th-order Runge-Kutta integrator (RK78) is implemented to precisely detect the switching time while maintain computational efficiency. For brevity, denote variable RK78 of each integration step as below

$$[\boldsymbol{y}_{k+1}, h_f, h_p] = RK78\_variable\_step(@\boldsymbol{f}', \boldsymbol{y}_k, t_k, h_g, tol) \tag{40}$$

and the fixed step RK78 within each step is given

$$[\boldsymbol{y}_{k+1}] = RK78\_fixed\_step(@\boldsymbol{f}', \boldsymbol{y}_k, t_k, h) \tag{41}$$

In Eq. (40), $@\boldsymbol{f}'$ represent the canonical equations as shown in Eq. (27). tol denote the integration tolerance, h_g is the current integration interval, h_f is the output step size which meet the integration tolerance and h_p is the prediction of step size in the next step. A brief introduction of variable RK78 is given as follows, during each step 7th and 8th-order approximations of the solution are calculated and compared. If the two answers do not agree to a specified tolerance, the step size is reduced, if the answers agree to more significant digits than required, the step size is increased. For energy optimal problem, as shown in Fig. 2, dividing the range of switching function into three intervals (∞, ε) , $[-\varepsilon, \varepsilon]$ and $(-\varepsilon, -\infty)$, which corresponding to the three different cases of u^* (i.e., Thrust turn 'Off', 'Medium' or 'On'). Within integration interval $[t_k, t_{k+1}]$, if the optimal thrust magnitude changes form 'On' to 'Medium' or from 'Medium' to 'On', the switching time t_{sw} must be precisely captured which makes $S(t_{sw}) = -\varepsilon$, similarly when the thrust magnitude changes form 'Off' to 'Medium' or from 'Medium' to 'Off', the switching time must precisely satisfy $S(t_{sw}) = \varepsilon$. In order to implement the Newton method, define the shooting function as $f(t_{sw}) = S(t_{sw}) + \varepsilon = 0$ or $f(t_{sw}) = S(t_{sw}) - \varepsilon = 0$. Suppose the start point of Newton algorithm equivalent to t_k, denote h_{sw} as the distance from t_k to the switching point and set its initial value to zero. The pseudo code are given as follow

- DO WHILE $(propagations < propagations_{max})$
  1. propagations = propagations + 1
  2. $h_{temp} = -f(t_{sw})/\dot{S}(t_{sw})$
  3. $h_{sw} = h_{sw} + h_{temp}$
  4. integrate the dynamics with fixed step RK78, i.e., $[\boldsymbol{y}_{sw}] = RK78\_fixed\_step(@\boldsymbol{f}', \boldsymbol{y}_k, t_k, h_{sw})$
  5. update $f(t_{sw})$ and $\dot{S}(t_{sw})$ with $\boldsymbol{y}_{sw}$
  6. IF $f(t_{sw}) < tolerance$

     exit Newton detection

     END IF
- END DO
- IF $f(t_{sw}) < tolerance$ AND $0 < h_{sw} < (t_{k+1} - t_k)$ (i.e., The predefined tolerance is satisfied and the switching point located between $[t_k, t_{k+1}]$)

  return the results

ELSE (i.e., The Newton method failed)

start bisection method to catch t_{sw}

- END IF

Noted that fixed step RK78 only used for detecting switching points. Through numerical simulation, if the Newton method succeed, the shooting function will reach machine precision (i.e., 10^{-15}) with only 4-5 iterations, if the Newton method failed because of the poor start point, bisection process will start and about 50 iterations are needed. Next, the detailed integration procedure of each step can be illustrated as below. Suppose among the $k-$th iterations, there are three cases with respect to S_k, for each of which there are also three cases with respect to S_{k+1}, the initial integration dynamics can be determined by the category of S_k

1) $S_k < -\varepsilon$. The thruster begins on, then integrate the dynamics with variable step RK78 to evaluate S_{k+1}

   a. $S_{k+1} < -\varepsilon$. The thruster is always on within the time interval h_f, save the results and update the next step size with h_p

   b. $-\varepsilon \leq S_{k+1} \leq \varepsilon$. The engine is first 'On' and then turn 'Medium' within h_f, catch the switching point with Newton and bisection method, update the state-transition-matrix, then modify the propagation maker of next step from 'On' to 'Medium'

   c. $S_{k+1} > \varepsilon$.

      IF $\varepsilon = 0$ (i.e., fuel-optimal problem)

         The engine is first 'On' and then turn 'Off', catch the switching point and update the state-transition-matrix, then modify the propagation maker of next step from 'On' to 'Off'

      ELSE

         The time interval is too big, go back and decrease the time interval h by half

      END IF

2) $-\varepsilon \leq S_k \leq \varepsilon$. The thruster begins medium, then propagate the dynamics with variable step RK78 to evaluate S_{k+1}

   a. $S_{k+1} < -\varepsilon$. The thruster is first 'Medium' and then 'On' within time interval h_f, detect the switching point and update the state-transition-matrix, at last convert integration marker from 'Medium' to 'On'

   b. $-\varepsilon \leq S_{k+1} \leq \varepsilon$. The engine is always 'Medium' within time interval h_f, save the results and update the next interval with h_p

   c. $S_{k+1} > \varepsilon$. The thruster is first 'Medium' and then turn 'Off' within time step h_f, first detect the switching point, followed by updating the state-transition-matrix, at the end change the integration marker from 'Medium' to 'Off'

3) $S_k > \varepsilon$. The thruster begins off, integrate the dynamics with variable step RK78 to evaluate S_{k+1}

   a. $S_{k+1} < -\varepsilon$.

IF $\varepsilon = 0$. (i.e., fuel-optimal problem)

The engine is first 'Off' and then turn 'On', catch the switching point and update the state-transition-matrix, then modify the propagation maker of next step from 'Off' to 'On'

ELSE

The time interval is too big, go back and decrease the time interval h by half

END IF

b. $-\varepsilon \leq S_{k+1} \leq \varepsilon$. The thruster is first 'Off' and then 'Medium' during the time interval h_f, capture the switching point and update the state-transition-matrix, at last change the propagation marker from 'Off' to 'Medium'

c. $S_{k+1} > \varepsilon$. The thruster is always 'Off' within time interval h_f, save the results and update the next interval with h_p.

Noted that the above integration process only suit for energy-optimal and fuel-optimal problems, but it can be used for time-optimal problem with little modifications.

SIMULATION AND RESULTS

The satellite is assumed to be initially on a GTO about the Earth, such orbit has perigee and apogee altitudes $h_p = 400km$ and $h_a = 35864km$ respectively, the transfer begins when the satellite is at the perigee and then orbital energy is increased by low thrust, the target is the first point on the halo orbit of Earth-Moon L_1, whose z amplitude equal to $8000km$. Tab. 1 summarizes the parameters used in this work, for computing convenience, the quantities about length, time, velocity and mass are non-dimensionalized by distance unit LU, time unit TU, velocity unit VU and mass unit MU respectively.

The aim of this work is to design fuel-optimal problem, but minimum time transfer should be calculated first in order to choose the final time $t_f \geq t_{f_{min}}$. It is hard to find an initialization of low thrust transfer trajectory directly, an effective idea is to introduce a discrete continuation on the maximal thrust magnitude T_{max}, (i.e., the thrust magnitude should reduce in decrease steps in order to link the easy problem to the difficult one.) This procedure is illustrated in Tab. 2, in this table, thrust force ranging from $10N$ to $0.3N$ and the corresponding time of flight increase from 7.8549 days to 171.6254 days. The final mass ratio are listed in the third column, it is interesting that the final mass ratio has minor changes (i.e., 0.8991 - 0.8462 = 0.0529, which equal to 5.29% of initial mass) even maximal thrust magnitude change dramatically (i.e., $10N$ to $0.3N$). For clarity, the time of flight and final mass ratio are plotted for different maximal thrust magnitude in Fig. 3. It can be seen that the final mass ratio increase monotonically from $10N$ to $1N$, and the fixed initial and final boundary condition maybe cause the final mass vibration below $1N$. Fig. 4 illustrates four typical transfer trajectory with respect to $10N$, $2N$, $1N$ and $0.6N$ respectively. And Fig. 5 shows the corresponding time history of thrust ratio, switching function and mass ratio respectively.

Once the minimum transfer time are solved for different maximum thrust magnitude, then we will focus on energy-optimal and fuel-optimal problems. In order to avoid the infinite transfer time problem, the time of flight is fixed and determined by a scalar $c_{tf} \times t_{fmin}$. Thrust magnitude homotopy is implemented first for the sake of lowest thrust magnitude of energy-optimal problem. It is mentioned that larger thrust magnitude exhibit bigger convergence radius and faster convergence speed, and if thrust magnitude homotopy is stuck, adjustment of c_{t_f} is a practical method to overcome

Table 1. Physical constants used in this work

Symbol	Value	Units	Meaning
μ	1.21506683×10^{-2}	—	Earth-Moon mass parameter
m_0	1500	kg	Initial mass of satellite
I_{sp}	3000	s	Specific impulse
g_0	9.80665	m/s^2	Gravitational acceleration
c	29.4199500	km/s	Exhaust velocity
LU	3.84405000×10^5	km	Distance unit
TU	3.75676967×10^5	s	Time unit
VU	1.02323281	km/s	Velocity unit
MU	1500	kg	Mass unit
h_p	400	km	perigee altitude
h_a	35864	km	apogee altitude
A_z	8000	km	z amplitude
$\boldsymbol{x}(t_0)$	-0.019488511458668	—	Initial position of x
	-0.016033479812051	—	Initial position of y
	0	—	Initial position of z
$\boldsymbol{v}(t_0)$	8.918881923678198	—	Initial velocity of v_x
	-4.081793688818725	—	Initial velocity of v_y
	0	—	Initial velocity of v_z
m_0	1	—	Initial mass
$\boldsymbol{x}(t_f)$	0.823385182067467	—	Final position of x
	0	—	Final position of y
	-0.022277556273235	—	Final position of z
$\boldsymbol{v}(t_f)$	0	—	Final velocity of v_x
	0.134184170262437	—	Final velocity of v_y
	0	—	Final velocity of v_z

Table 2. Different maximal thrust magnitude with respect to minimum final time and final mass ratio in time-optimal case.

$T_{max}(N)$	$t_{f_{min}}(days)$	m_{tf} (time-optimal)
10	7.8549	0.8462
9	8.6861	0.8469
8	9.6522	0.8488
7	10.8133	0.8518
6	12.6278	0.8516
5	12.9634	0.8730
4	16.0510	0.8742
3	21.1363	0.8758
2	29.1512	0.8858
1	56.2458	0.8898
0.9	59.8376	0.8945
0.8	64.6165	0.8987
0.7	80.2242	0.8900
0.6	87.6674	0.8970
0.5	112.0327	0.8903
0.4	138.4519	0.8915
0.3	171.6254	0.8991

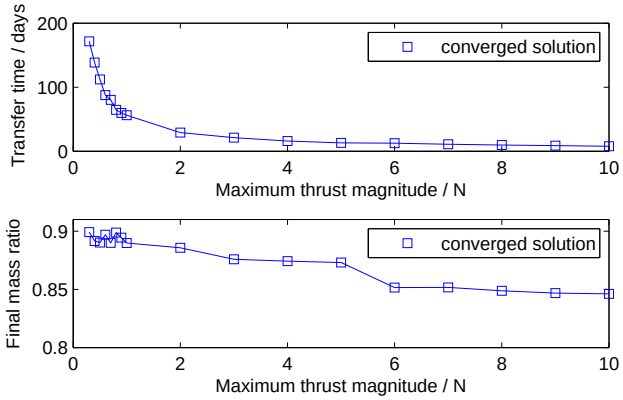

Figure 3. Maximal thrust magnitude versus transfer time and final mass ratio in the time-optimal problem

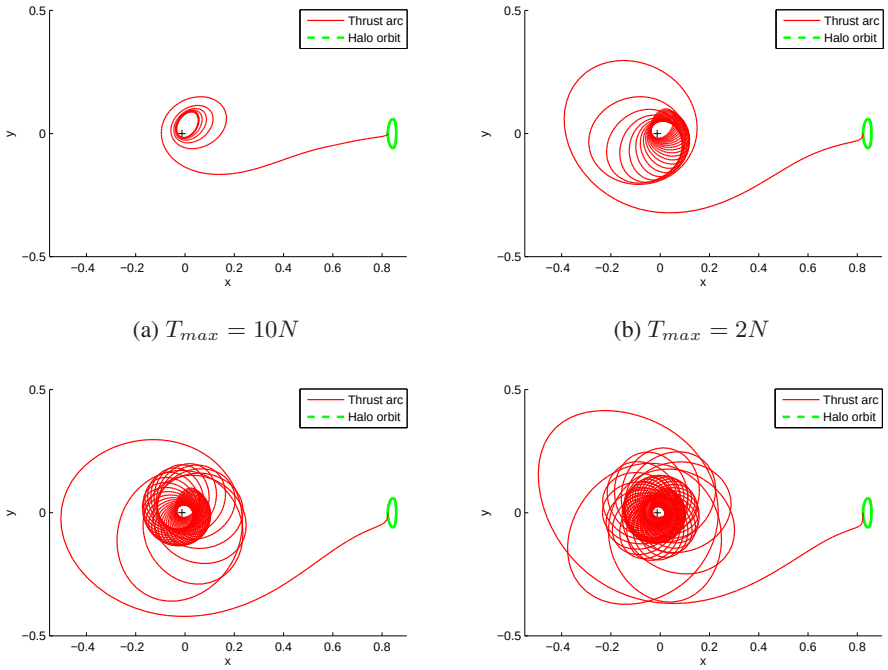

(a) $T_{max} = 10N$

(b) $T_{max} = 2N$

(c) $T_{max} = 1N$

(d) $T_{max} = 0.6N$

Figure 4. Time-optimal trajectories from GTO to L_1 with $10N$, $2N$, $1N$ and $0.6N$ respectively, CRTBP frame.

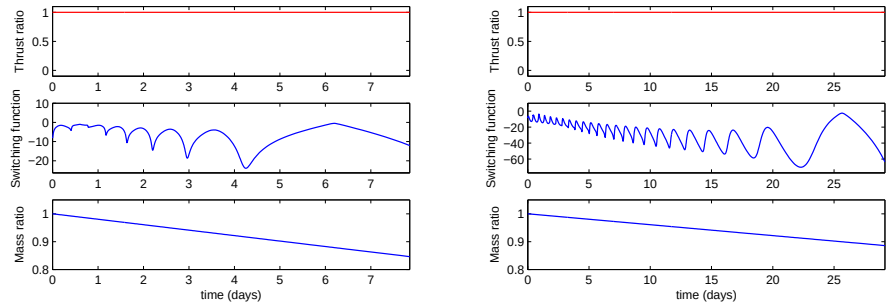

(a) $T_{max} = 10N$ (b) $T_{max} = 2N$

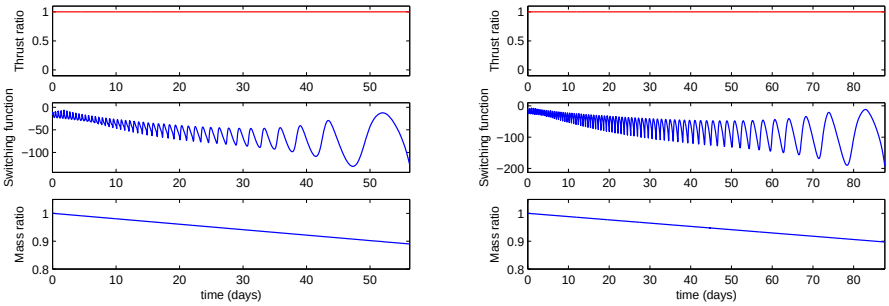

(c) $T_{max} = 1N$ (d) $T_{max} = 0.6N$

Figure 5. In time-optimal case, time history of thrust ratio, switching function and mass ratio corresponding to $10N$, $2N$, $1N$ and $0.6N$ respectively

convergence difficulty. Then, an other discrete energy-consumption homotopy[24,21] is implemented to convert energy-optimal to the corresponding fuel-optimal problem by adjusting the parameter ε of Eq. (5). Tab. 3 listed simulation results of thrust magnitude ranging from $10N$ to $0.6N$ with respect to final mass ratio of both energy-optimal and fuel-optimal cases. It can be concluded that fuel-optimal solutions have less fuel-consumption than the corresponding energy-optimal cases. In the $T_{max} = 0.6N$ solution, this transfer trajectory lasts 140.26 days (i.e., $1.6 \times t_{f_{min}}$), and the final mass ratio is 0.9150, which means compared with time-optimal problem, 27 kg fuel are saved with additional 52.59 days. Because energy-optimal and fuel-optimal problem is much more difficult to converge than time-optimal problem stated above, no solution found under $T_{max} = 0.6N$.

Four typical fuel-optimal transfer trajectories are shown in Fig. 6 under the synodic frame with maximal thrust level equal to $10N$, $2N$, $1N$ and $0.6N$ respectively. And Fig. 7 illustrates the same transfer trajectories in Earth centered inertial frame. In both two figures, the thick red line shows the thrust arcs, the thin blue line represents the coast arcs and the dash green line is halo orbit around L_1. It can be concluded from the four cases, the thruster is on duty near the periapses and turn off near the apoapsis. Because the fixed transfer time and the asymptotic property of stable manifold, a short maneuver is needed to insert the satellite into the halo orbit in the last spiral. Fig. 8 shows the profile of thrust magnitude, time history of switching function and mass ratio, respectively. In Fig. 8d, the control profile has about 150 bang-bang structures.

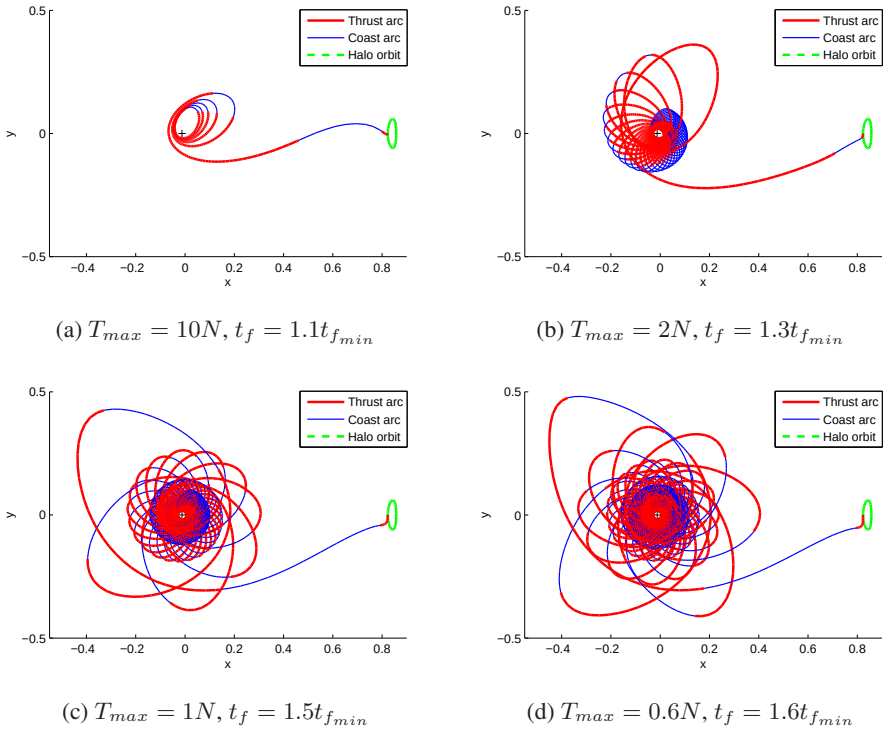

(a) $T_{max} = 10N$, $t_f = 1.1t_{f_{min}}$

(b) $T_{max} = 2N$, $t_f = 1.3t_{f_{min}}$

(c) $T_{max} = 1N$, $t_f = 1.5t_{f_{min}}$

(d) $T_{max} = 0.6N$, $t_f = 1.6t_{f_{min}}$

Figure 6. Fuel-optimal trajectories from GTO to L_1 with $10N$, $2N$, $1N$ and $0.6N$ respectively, CRTBP frame.

Table 3. Different maximal thrust magnitude with respect to final mass ratio of both energy-optimal and fuel-optimal cases

$T_{max}(N)$	c_{t_f}	t_f	m_{tf} (energy-optimal)	m_{tf} (fuel-optimal)
10	1.1	8.6404	0.9034	0.9105
9	1.1	9.5548	0.9016	0.9103
8	1.1	10.6174	0.9003	0.9090
7	1.1	11.8946	0.8988	0.9072
6	1.2	15.1533	0.9009	0.9092
5	1.3	16.8524	0.8964	0.9053
4	1.3	20.8663	0.8936	0.9015
3	1.3	27.4773	0.8992	0.9088
2	1.3	37.8965	0.9091	0.9146
1	1.5	84.3688	0.9038	0.9131
0.8	1.75	113.0789	0.9076	0.9174
0.6	1.6	140.2678	0.9069	0.9150

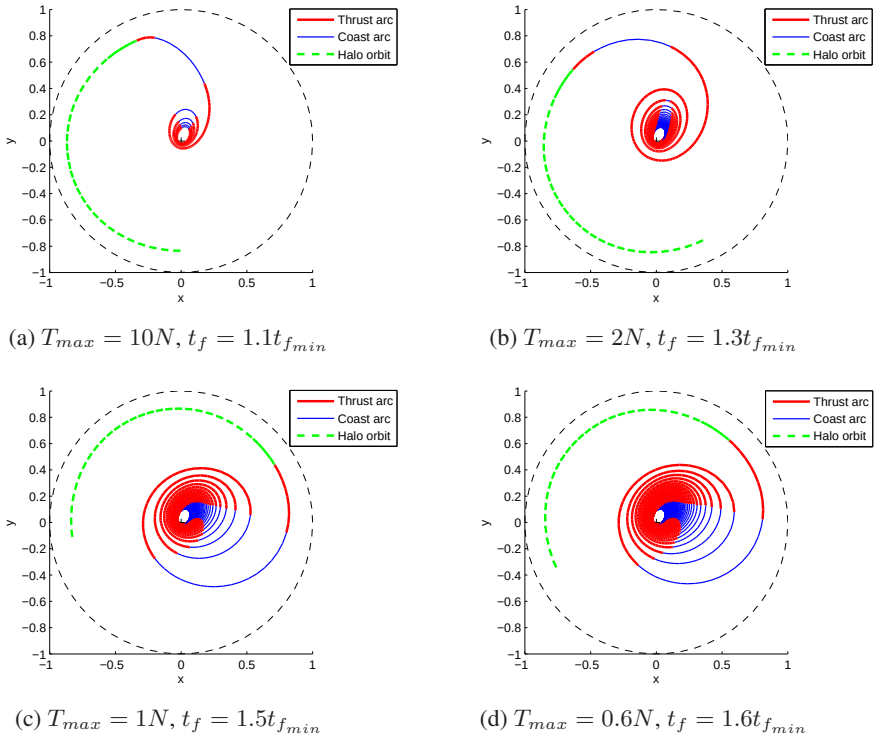

(a) $T_{max} = 10N$, $t_f = 1.1t_{f_{min}}$

(b) $T_{max} = 2N$, $t_f = 1.3t_{f_{min}}$

(c) $T_{max} = 1N$, $t_f = 1.5t_{f_{min}}$

(d) $T_{max} = 0.6N$, $t_f = 1.6t_{f_{min}}$

Figure 7. Time-optimal trajectories from GTO to L_1 with $10N$, $2N$, $1N$ and $0.6N$ respectively, Earth centered inertial frame.

CONCLUSION

In this work, fuel-optimal trajectories from the Earth to the Earth-Moon L_1 halo orbit is investigated by indirect method with constant specific impulse engines. Several techniques are used to improve sensitivity and efficiency caused by the highly nonlinear dynamics and discontinuous control profile. Homotopic method is implemented to solve fuel-optimal problem start from a related and easier energy-optimal problem. The analytical derivatives of constraints with respect to initial variables are derived analytically for both fuel-optimal problem and energy-optimal problem, and a combination of Newton and bisection method is proposed to efficiently detect the switching point. A low thrust transfer trajectory from GTO to halo orbit around Earth-Moon L_1 point is used to test those techniques stated above, the difficult fuel-optimal low thrust transfer problem are divided into two sub-problems, first time-optimal problem is solved to give the minimum time-of-flight of the subsequent energy-optimal problem, then fuel-optimal problem is solved start from the converged solution given by energy-optimal problem. The simulations turns out to be efficient when applied to 3-body models where the highly non-linearities ask for the very low thrust transfers.

ACKNOWLEDGMENT

C.Z. would like to acknowledge the Chinese Scholarship Council (CSC) which financially supported his visit to Politecnico di Milano.

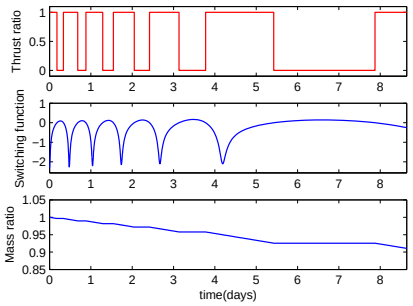

(a) $T_{max} = 10N$, $t_f = 1.1t_{f_{min}}$

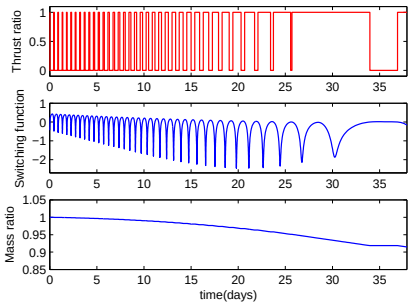

(b) $T_{max} = 2N$, $t_f = 1.3t_{f_{min}}$

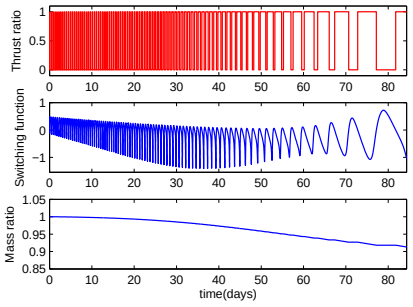

(c) $T_{max} = 1N$, $t_f = 1.5t_{f_{min}}$

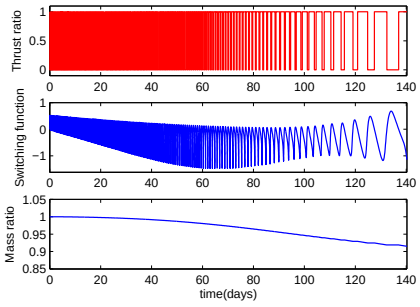

(d) $T_{max} = 0.6N$, $t_f = 1.6t_{f_{min}}$

Figure 8. In fuel-optimal case, time history of thrust ratio, switching function and mass ratio corresponding to $10N$, $2N$, $1N$ and $0.6N$ respectively

REFERENCES

[1] R. W. Farquhar *et al.*, "The flight of ISEE-3/ICE: origins, mission history, and a legacy," *Journal of the Astronautical Sciences*, Vol. 49, No. 1, 2001, pp. 23–74.

[2] G. GOMEZ, A. JORBA, J. MASDEMONT, and C. Simó, "A dynamical systems approach for the analysis of the SOHO mission," *ESA, Spacecraft Flight Dynamics p 449-454(SEE N 92-24719 15-12)*, 1991.

[3] E. Stone, L. Burlaga, A. Cummings, W. Feldman, W. Frain, J. Geiss, G. Gloeckler, R. Gold, D. Hovestadt, S. Krimigis, *et al.*, "The advanced composition explorer," *AIP Conf. Proc*, Vol. 203, 1989, pp. 48–58.

[4] C. L. Bennett, M. Bay, M. Halpern, G. Hinshaw, C. Jackson, N. Jarosik, A. Kogut, M. Limon, S. Meyer, L. Page, *et al.*, "The microwave anisotropy probe mission," *The Astrophysical Journal*, Vol. 583, No. 1, 2003, p. 1.

[5] M. W. Lo, B. G. Williams, W. E. Bollman, D. Han, Y. Hahn, J. L. Bell, E. A. Hirst, R. A. Corwin, P. Hong, K. C. Howell, *et al.*, "Genesis mission design," *Journal of the Astronautical Sciences*, Vol. 49, No. 1, 2001, pp. 169–184.

[6] M. D. Rayman, P. Varghese, D. H. Lehman, and L. L. Livesay, "Results from the Deep Space 1 technology validation mission," *Acta Astronautica*, Vol. 47, No. 2, 2000, pp. 475–487.

[7] J. Kugelberg, P. Bodin, S. Persson, and P. Rathsman, "Accommodating electric propulsion on SMART-1," *Acta Astronautica*, Vol. 55, No. 2, 2004, pp. 121–130.

[8] H. Kuninaka, K. Nishiyama, I. Funaki, T. Yamada, Y. Shimizu, and J. Kawaguchi, "Asteroid rendezvous of hayabusa explorer using microwave discharge ion engines," *29th International Electric Propulsion Conference, number IEPC-2005-10*, 2005.

[9] A. E. Bryson, *Applied optimal control: optimization, estimation and control*. CRC Press, 1975.

[10] J. T. Betts, "Survey of numerical methods for trajectory optimization," *Journal of guidance, control, and dynamics*, Vol. 21, No. 2, 1998, pp. 193–207.

[11] J. Riehl, S. Paris, and W. Sjauw, "Comparison of implicit integration methods for solving aerospace trajectory optimization problems," *AIAA/AAS Astrodynamics Specialist Conference and Exhibit*, 2006, pp. 21–24.

[12] L. Pontryagin, V. Boltyanskii, R. Gamkrelidze, and E. Mishchenko, *The Mathematical Theory of Optimal Processes*. John Wiley & Sons, New York, 1962.

[13] J. Senent, C. Ocampo, and A. Capella, "Low-thrust variable-specific-impulse transfers and guidance to unstable periodic orbits," *Journal of Guidance, Control, and Dynamics*, Vol. 28, No. 2, 2005, pp. 280–290.

[14] M. Ozimek and K. Howell, "Low-thrust transfers in the Earth-Moon system, including applications to libration point orbits," *Journal of Guidance, Control, and Dynamics*, Vol. 33, No. 2, 2010, pp. 533–549.

[15] G. Mingotti, F. Topputo, and F. Bernelli-Zazzera, "Low-Energy, Low-Thrust Transfers to the Moon," *Celestial Mechanics and Dynamical Astronomy*, Vol. 105, November 2009, pp. 61–74, 10.1007/s10569-009-9220-7.

[16] G. Mingotti, F. Topputo, and F. Bernelli-Zazzera, "Efficient Invariant-Manifold, Low-Thrust Planar Trajectories to the Moon," *Communication in Nonlinear Science and Numerical Simulation*, Vol. 17, No. 2, 2012, pp. 817–831, 10.1016/j.cnsns.2011.06.033.

[17] G. Mingotti, F. Topputo, and F. Bernelli-Zazzera, "Combined Optimal Low-Thrust and Stable-Manifold Trajectories to the Earth–Moon Halo Orbits," *AIP Conference Proceedings*, Vol. 886, February 2007, pp. 100–110, 10.1063/1.2710047.

[18] J.-B. Caillau and B. Daoud, "Minimum time control of the restricted three-body problem," *SIAM Journal on Control and Optimization*, Vol. 50, No. 6, 2012, pp. 3178–3202.

[19] R. P. Russell, "Primer vector theory applied to global low-thrust trade studies," *Journal of Guidance, Control, and Dynamics*, Vol. 30, No. 2, 2007, pp. 460–472.

[20] W. S. Koon, M. W. Lo, J. E. Marsden, and S. D. Ross, "Dynamical systems, the three-body problem and space mission design," 2000.

[21] T. Haberkorn, P. Martinon, and J. Gergaud, "Low thrust minimum-fuel orbital transfer: a homotopic approach," *Journal of Guidance, Control, and Dynamics*, Vol. 27, No. 6, 2004, pp. 1046–1060.

[22] B. A. Conway, *Spacecraft trajectory optimization*, Vol. 32. Cambridge University Press, 2010.

[23] F. Jiang, H. Baoyin, and J. Li, "Practical techniques for low-thrust trajectory optimization with homotopic approach," *Journal of Guidance, Control, and Dynamics*, Vol. 35, No. 1, 2012, pp. 245–258.

[24] R. Bertrand and R. Epenoy, "New smoothing techniques for solving bang–bang optimal control problemsnumerical results and statistical interpretation," *Optimal Control Applications and Methods*, Vol. 23, No. 4, 2002, pp. 171–197.

[25] J. R. Stuart, *FUEL-OPTIMAL, LOW-THRUST TRANSFERS BETWEEN LIBRATION POINT ORBITS*. PhD thesis, Purdue University, 2011.

[26] Lawden, *Optimal Trajectories for Space Navigation*. Butterworths, London, 1963.